International Journal of Computational and Experimental Science and ENgineering (IJCESEN)

Vol. 11-No.4 (2025) pp. 10025-10034
http://www.ijcesen.com

ISSN: 2149-9144

Research Article

Elaboration and Characterization of Ni-Zn Thin Films on AICI 430 stainless steel by Co-Sputtering Magnetron

Samy Anas[1*], Naima Zaourar Boutarek[2], Philippe David[3], Eric Mossang[4], Samir Mansour[5], Faouzi Messaoud[6]

[1]University of Sciences and Technology Houari Boumediene USTHB, Laboratory of Materials Technologies.B.P. 2 El Alia, Bab Ezzouar, Alger, Algeria.
*** Corresponding Author Email:** anas.samy.sdm@gmail.com - **ORCID:** 0009-0009-7641-1440

[2]University of Sciences and Technology Houari Boumediene USTHB, Laboratory of Materials Technologies. B.P. 2 El Alia, Bab Ezzouar, Alger, Algeria.
Email: naima.boutarek@gmail.com - **ORCID:**0009-0007-3775-8711

[3]Institut Néel, CNRS UPR2940, 25 avenue des Martyrs BP 166 38042 Grenoble cedex 9
Email: philippe.david@neel.cnrs.fr. - **ORCID:** 0000-0003-4748-9715

[4]Institut Néel, CNRS UPR2940, 25 avenue des Martyrs BP 166 38042 Grenoble cedex 9
Email: eric.mossang@neel.cnrs.fr - **ORCID:** 0000-0003-0084-4660

[5]University of Sciences and Technology Houari Boumediene USTHB, Laboratory of Materials Technologies. B.P. 2 El Alia, Bab Ezzouar, Alger, Algeria.
Email: mansourusthb@yahoo.fr - **ORCID:** 0009-0003-4320-6594

[6]University of Sciences and Technology Houari Boumediene USTHB, Laboratory of Materials Technologies. B.P. 2 El Alia, Bab Ezzouar, Alger, Algeria.
Email: faouzi_messaoud@yahoo.com - **ORCID:** 0009-0009-9276-7519

Article Info:

DOI: 10.22399/ijcesen.4539
Received: 03 September 2025
Revised: 10 December 2025
Accepted: 15 December 2025

Keywords
Co sputtering magnetron,
Stainless steel,
Nickel-Zinc
Characterization,
Thin film

Abstract:

By serving as a catalyst and boosting reaction efficiency in procedures like water electrolysis, biomass gasification, and photochemical reactions, nickel-based component plays a crucial part in the production of hydrogen. The purpose of this work was to use Magnetron Sputtering technology to develop nickel-zinc thin films on a stainless-steel substrate. Scanning electron microscopy, XPS spectroscopy, X-ray diffraction, and the electron probe micro-analyzer (EPMA) were used to examine the surface morphology, crystal structure, and chemical composition of the Ni-Zn thin films respectively.
According to the found results, we confirm that the Nickel Zinc thin film was well deposited on stainless steel and it can be applied on different application especially on hydrogen production.

1. Introduction

Because of their many active sites and configurable electronic structures, transition metal-based catalysts (Fe, Ni, Co, and Cu) have recently drawn interest as affordable substitutes with superior activity and tunable selectivity [1-3]. Nickel–Zinc alloy coatings are being examined for their superior corrosion resistance compared to zinc coatings, particularly in electrical as Ni-Zn battery [4-6] and construction applications, as well as for aluminium alloy coatings. These coatings serve as viable substitutes for cadmium, which is highly toxic; thus, environmental regulations promote the adoption of alternative protective systems due to health and pollution concerns. Apart from their employment in steel automobile bodies [7, 8], nickel-zinc alloy coatings are also being evaluated for use in electrical catalysts [9–11], steel wire connections [12], and electronics [13]. Additionally, nickel-zinc alloy coatings are utilized in conjunction with chromate or other coatings [14-17]. Nickel-based catalysts are studied for both the anode and cathode sides of the electrolysis process in the literature that is currently

available. NiCo2Px [18], PtNi-decorated Ni [19], and PtNiO on carbon [20] for the cathode side and NiFe2Ox [21], IrNi [22], and IrNiCu [23] for the anode side are some of the catalysts that were investigated to evaluate the electrolysis performance. Researchers are increasingly interested in using transition group metals, such Ni, Zn and Fe, to create electrocatalysts because of their affordability, which stems from their abundance on Earth [24]. Based on our knowledge. No paper about nickel– zinc coating by co sputtering magnetron was reported in the literature. In this paper, a deep characterization of Ni-Zn thin film layer deposited by co sputtering magnetron is reported.

2. Material and Methods

2.1. Ni-Zn thin film deposition

The Ni-Zn thin films were deposited on several pieces of 430 stainless steel and silicon substrate by RF magnetron Co-sputtering system at 250°C. Prior to the deposition, the stainless-steel and silicon substrates underwent ultrasonic cleaning in acetone followed by ethanol at 50 °C, after which they were rinsed with deionized water and dried under a nitrogen stream to ensure surface cleanliness and reproducibility of the sputtering process. The Ni–Zn thin films were deposited onto 430 stainless-steel substrates by RF magnetron co-sputtering (Fig.1). In addition, selected films were deposited under identical conditions onto silicon (Si) substrates for subsequent characterization. Three different chemical compositions were deposited: Ni–Zn (50/50 at%) and Ni–Zn (75/25 at%) with a thickness of 1 µm. All depositions were conducted in a high-purity argon atmosphere with a constant flow rate of 10^{-2} sccm, a target–substrate separation of 8 cm, and a base pressure of 10^{-8} mbar. The sputtering power applied to the individual targets was adjusted according to the desired film composition, namely 60 W (Ni) / 20 W (Zn) for the 50/50 at% films and 80 W (Ni) / 10 W (Zn) for the 75/25 at% film. The corresponding deposition durations were 3000 s for both 1 µm films, all performed at a substrate temperature of 250 °C. All the condition of the deposition films was presented on the table 1.

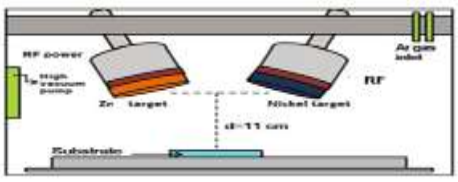

Figure.1. *RF magnetron Co-sputtering [25]*

2.2. Ni -Zn thin film characterizations

The chemical composition was determined by Electron Probe Micro Analysis (EPMA) Jeol JXA 8230 with a minimum of three measurements. XRD experiments were conducted on a Philips X'Pert instrument with CuKa radiation (l = 0.15418 nm). The morphology of the thin film was observed using a scanning electron microscope type JSM- 7610F Plus and the chemical composition was confirmed by EDS analysis. To explore the elemental composition of the surface and the oxidation states of the chemical elements forming our deposit, a characterization by XPS « Escalab 250 Xi » was performed.

3. Results and Discussions

3.1. Chemical composition determination by EPMA

To confirm the chemical composition of our thin films, two measurements by EPMA were carried out for the thin films deposited.

3.1.1. Ni-Zn 75/25

The Fig.2 shows the two different positions selected on the 75/25 Ni-Zn thin layer and the representative's peaks elements of these compositions. The Table 2. represents the chemical composition of the deposited Ni-Zn films for the two positions. Based on the results reported in Figure 1 and Table 2. These analyses confirm that the layer deposited by Magnetron Co-sputtering has a Ni composition very close to that targeted. The chemical elements of the substrate, Fe and Cr, are also detected, because EPMA is a volume analysis technique. It is probably the presence of these elements in the calculation of the overall composition of the layer that is at the origin of the observed shift in the Zn content. Disregarding these elements, we confirm that the deposited layer is of the Nickel/Zinc type with a concentration of 75%/25% respectively.

3.1.2. Ni-Zn 50/50

The Fig.2 shows the two different positions selected on the 50/50 Ni-Zn thin layer and the representative's peaks of these compositions. The Table 3. represents the chemical composition of the deposited Ni-Zn films for the two positions. Following chemical analysis by EPMA, it is confirmed that the layer deposited by Magnetron Co-sputtering is indeed a layer consisting of 50% Nickel (the most intense peak). As in the case of the Ni-Zn deposit (75/25), the chemical elements of the substrate Fe and Cr appear in the chemical composition, and their presence is probably

responsible for the shift in the zinc concentration compared to the target one. By ignoring these elements, it is confirmed that the chemical composition of the Ni-Zn deposited layer is in conformity with the target composition.

3.2. X ray diffraction

3.2.1 Ni-Zn 75/25

The results of the X-ray diffraction (Fig. 4 and Table. 4) reveal, in addition to the (100) peak of the silicon used as a substrate for some cases of deposits intended for structural characterizations and not for hydrogen production, the (101), (200), and (600) peaks of the Ni-Zn phase.

Table 1. *The conditions of the deposited Ni-Zn films*

Target Layer Composition	Ar Flow Rate [sccm] (100% Ar)	Distance [cm]	Base Pressure [mbar]	Power [W]	Deposition Time [s]	Deposition Temperature (°C)
Ni–Zn (50/50 at%) 1 µm	10	8	10^{-8}	Ni 60 / Zn 20	3000	250
Ni–Zn (75/25 at%) 1 µm	10	8	10^{-8}	Ni 80 / Zn 10	3000	250

Table 2. *Chemical composition of the deposited 75/25 Ni-Zn films*

Chemical composition position 1

Element	Weight (%)	Atomique (%)
Cr	0.766	0.8499
Ni	77.995	76.7088
Zn	14.822	13.0920
Fe	5.363	5.5448
O	1.054	3.8046
Total	100.000	100.0000

Chemical composition position 2

Elements	Weight (%)	Atomique (%)
Cr	0.976	1.0771
Ni	77.408	75.6491
Zn	14.731	12.9305
Fe	5.606	5.7595
O	1.279	4.5837
Total	100.000	100.0000

Table.3 *Chemical composition of the deposited Ni-Zn 50/50 films*

Chemical composition position 1

Element	Weight (%)	Atomique (%)
Cr	5.187	3.2607
Ni	49.126	49.23
Zn	21.562	19.4055
Fe	23.067	24.2990
O	1.055	3.8048
Total	100.000	100.0000

Chemical composition position 2

Element	Weight (%)	Atomique (%)
Cr	5.187	3.2607
Ni	50.126	50.43
Zn	21.562	19.4055
Fe	22.067	23.0990
O	1.055	3.8048
Total	100.000	100.0000

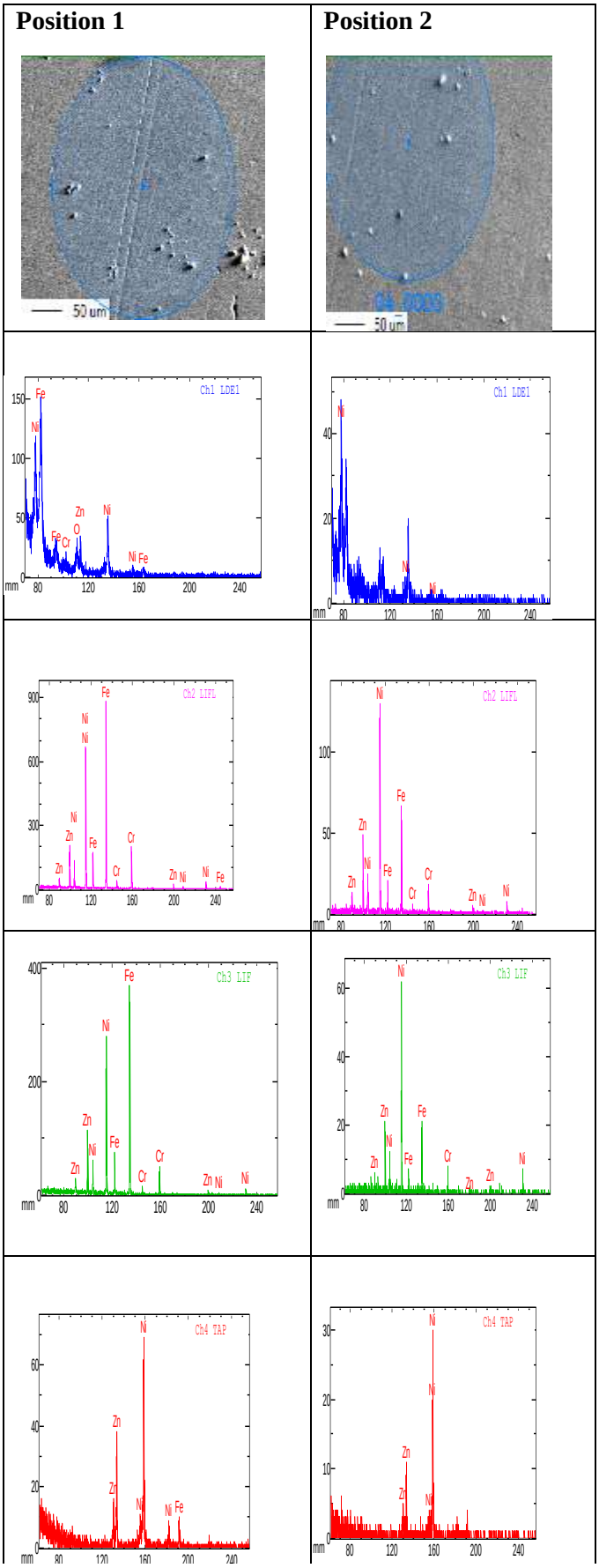

Figure 2. *75/25 Ni-Zn micrograph and representative elements peaks by EPMA*

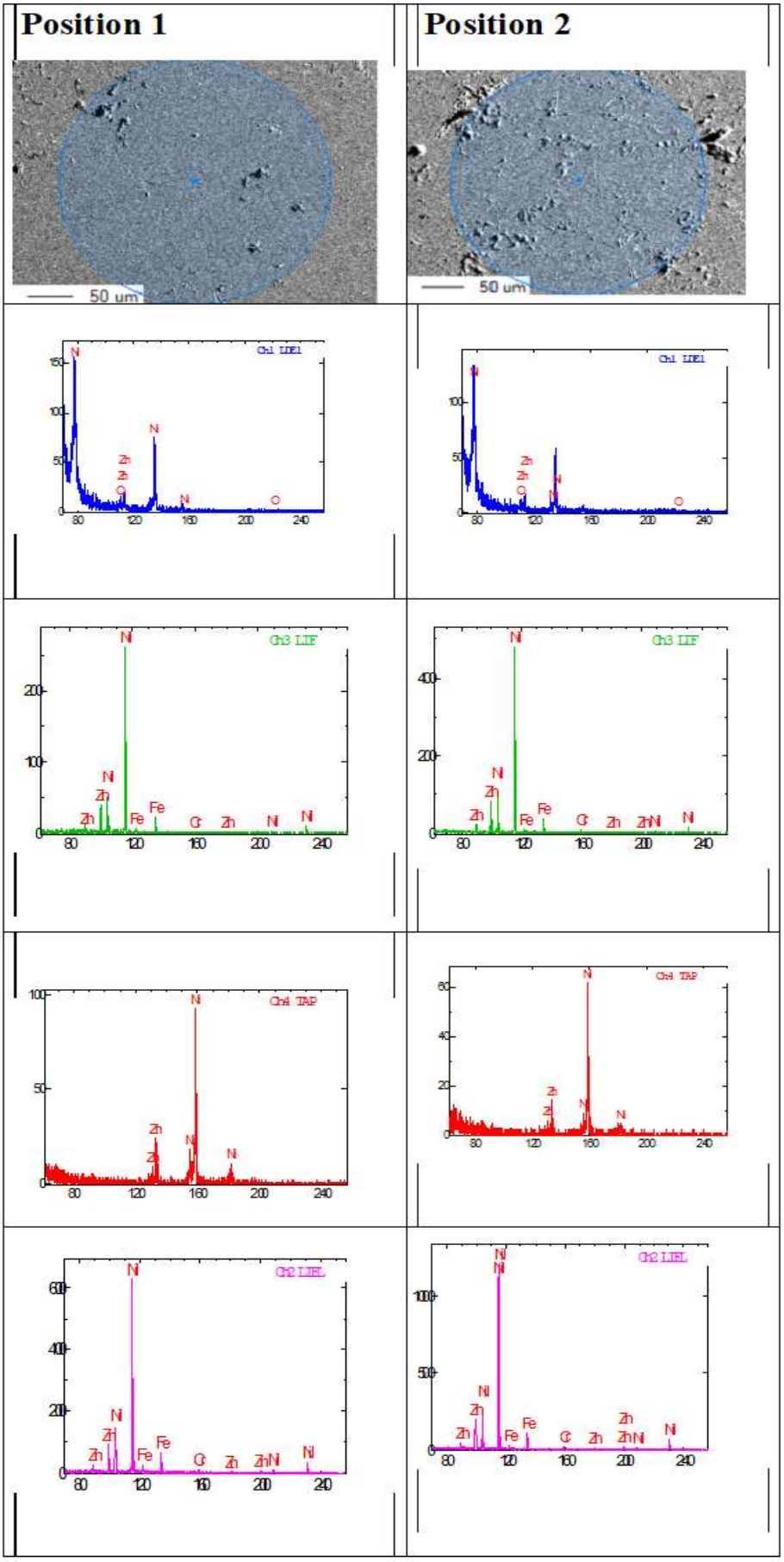

Figure 3. *50/50 Ni-Zn micrograph and representative elements peaks by EPMA*

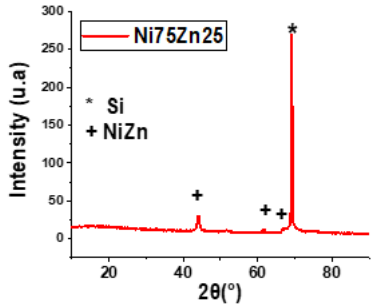

Figure 4. *XRD spectrum of 75/25 Ni-Zn*

Table 4. *XRD peaks of 75/25 Ni-Zn*

2θ (°)	d	hkl	peak	Ref
44,25	2,053	101	NiZn	[26,27]
64	1,443	200	NiZn	[27,28]
68	1,502	600	NiZn	[27,29]
69,3	1,37	100	Silicon	[30]
69,5	1,354	103	Zinc	[31,32]

Table 5. *XRD peaks of 50/50 Ni-Zn*

2θ (°)	d	hkl	peak	Ref
44,25	2,052	101	NiZn	[26,27]
64	1,435	200	NiZn	[27,28]
68	1,502	600	NiZn	[27,28]
69,3	1,354	100	Silicon	[29]
69,5	1,354	103	Zinc	[30,31]

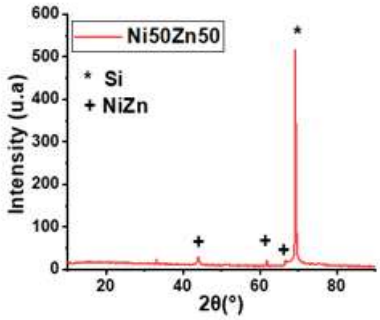

Figure 5. *XRD spectrum of 50/50 Ni-Zn*

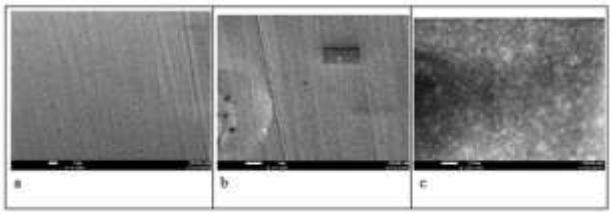

Figure .6 *SEM microphotographs of the surface of Ni-Zn (75/25) deposits observed at different magnifications a) x5000, b) x10000 and c) x10000*

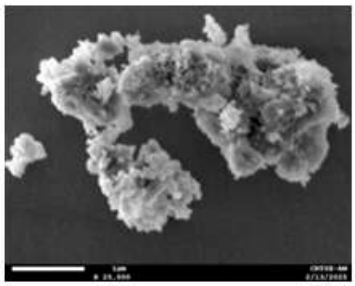

Figure.7 *SEM micrograph of a grain on the Ni-Zn (75/25) deposition surface with 3D growth*

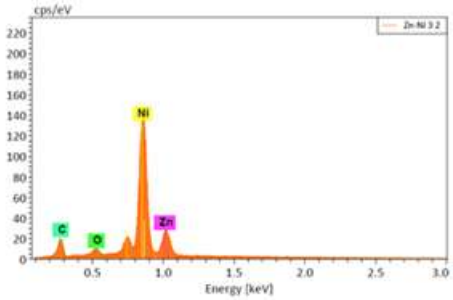

Figure .8 *EDS Analysis 75/25 Ni-Zn*

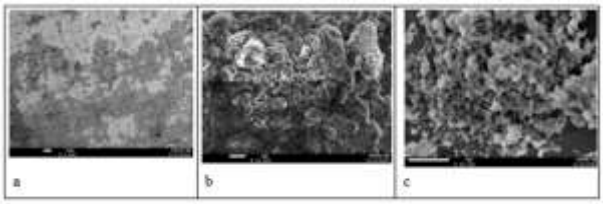

Figure .9 *SEM microphotographs of the surface of Ni-Zn (50/50) deposits observed at different magnifications a) x5000, b) x10000 and c) x25000.*

Table 6. *Chemical composition by EDS analysis75/25 Ni-Zn*

Element	Weight [%]	Atomique [%]
Nickel	77,94	65,8
Zinc	16,37	12,41
Carbone	4,06	16,75
Oxygene	1,63	5,05
Total	100	100

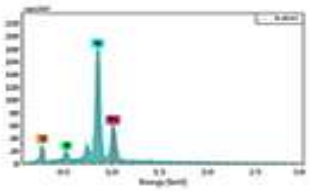

Figure .10 EDS Analysis 50/50 Ni-Zn

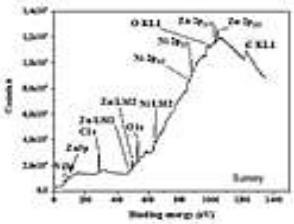

Figure .11 XPS analysis / Survey Ni-Zn 75/25

Table 7. Chemical composition by EDS analysis 50/50 Ni-Zn

Element	Weight [%]	Atomique [%]
Nickel	68,28	56,08
Zinc	24,62	18,15
Carbone	4,35	17,48
Oxygene	2,75	8,29
Total	100	100

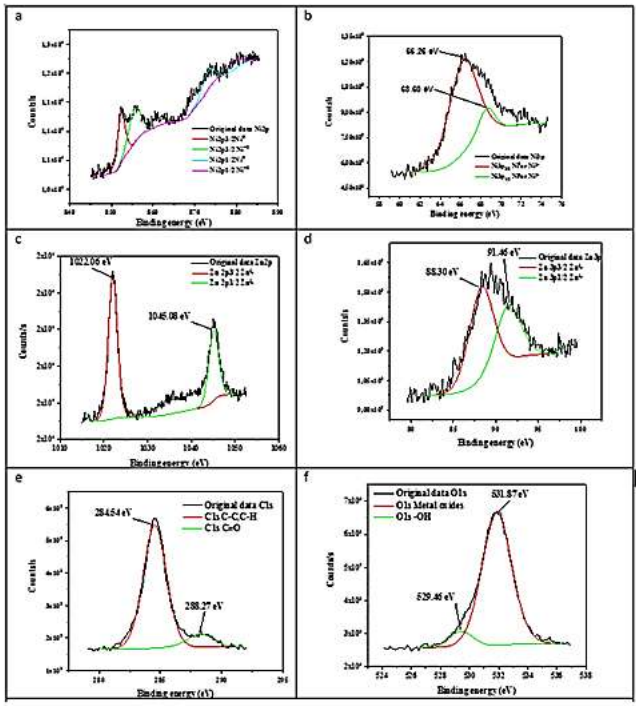

Figure .12 *XPS analysis Ni-Zn 75/25* a)Ni2p, b)Ni3p ,c) Zn2p, d) Zn3p, e) C1s , f) O2s

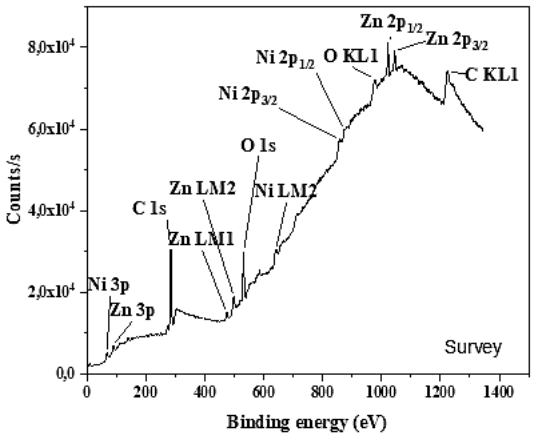

Figure .13 *XPS analysis/Survey Ni-Zn 50/50*

3.2.2 Ni-Zn 50/50

As previously mentioned, the results of the X-ray diffraction (Fig5 and Table 5) reveal, in addition to the (100) peak of the silicon used as a substrate, the (101), (200), and (600) peaks of the Ni-Zn phase.

3.3 SEM micrograph

The morphology of the deposited Ni-Zn layer was carried out by scanning electron microscopy.

3.3.1 Ni-Zn 75/25

Detailed observation using a scanning electron microscope of the surface of the Ni-Zn (75/25)

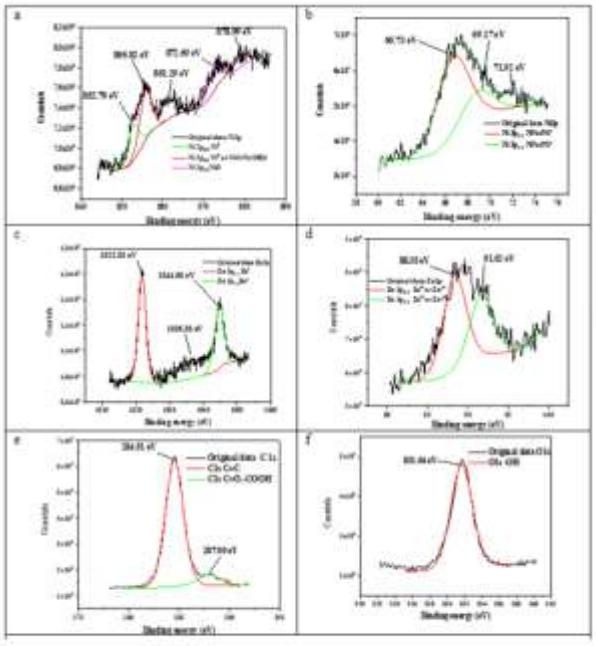

Figure .14 *XPS analysis Ni-Zn 50/50* a) Ni2p, b) Ni3p, c) Zn2p, d) Zn3p, e) C1s, f) O2s

deposit reveals at low magnification (Fig.6.a and 6.b) a relatively dense and uniform structure. At higher magnification (Fig.6c), the presence of a grain structure with two contrasts, light and gray, is highlighted. The measured grain size varies between 80 and 160 nm. Figure .7 shows a SEM micrograph of a grain on the Ni-Zn (75/25) deposition surface with 3D growth. According to the Fig.8 and Table. 6, the chemical composition is mainly composed of nickel (Ni) at 65.8 at. % and Zn at 12.41 at. Note that in this case, the ratio of the measured Ni/Zn composition remain acceptable compared to the target value.

3.3.2 Ni-Zn 50/50

Detailed observation with a scanning electron microscope of the surface of the Ni-Zn (50/50) deposit reveals at low magnification (Fig.9a) a relatively dense and uniform structure. The presence of two light and gray contrasts can be distinguished, which can be attributed to a two-phase structure. At higher magnification (Fig.9b and 9c), grains with a size between 60 and 180 nm are highlighted. These have an angular morphology and develop a three-dimensional growth. Furthermore, the chemical composition of a grain determined by energy dispersive spectrometry (EDS) (Fig.10 and Table .7) shows that the Ni-Zn (50/50) deposit is mainly composed of nickel (Ni) at 56.08 at. %, and zinc (Zn) at 18.15 at. %. Note that the measured Ni content closely corresponds to the expected composition, while that of Zn deviates significantly from it.

3.4 XPS analysis

3.4.1 Ni-Zn 75/25

To explore the elemental composition of the surface and the oxidation states of the chemical elements forming our deposit (extreme surface), a characterization by XPS was performed. Figures .11 and .12 present the wide-range energy scan spectra (from 0 to 1500 eV) of the Ni-Zn samples (75/25) included all revelated peaks [32,33]. The high-resolution Ni 2p spectrum shows two sets of peaks at 855.82and 872.5 eV with their respective satellites, which correspond to the 2p3/2 and 2p1/2 levels, respectively. Also, the 3p peaks of NiII are observed at 67.3 eV and 71.92 eV [34]. As shown in Figure 4a, the XPS spectrum of Zn 2p reveals the binding energies of Zn 2p3/2at about 1,021.8 eV and Zn 2p1/2 centered at 1045 eV [35].The XPS spectra reveals the Zn3p peak at 88.2 and 91.3 eV [36].The oxygen O1s with binding energy of (529.46 eV–531.87 eV) could be assigned and it was well known that the high amount of surface chemisorbed oxygen was enhancing the activity of the resulting catalyst [37]. Carbon 1s core-level lines attributed to C-C and C=O bindings are positioned at 284.54 and 288.27 eV,respectively[38].

3.4.2 Ni-Zn 50/50

Figures .13 and .14 present the wide-range energy scan spectra (from 0 to 1500 eV) of the Ni-Zn samples (50/50), showing the presence of the elements Ni, Zn, C, and O at their signature binding energy positions. The same XPS peaks regarding the Ni-Zn samples (75/25) are also observed on the Ni-Zn samples (50/50).

5. Conclusion

In the face of increasingly pressing environmental concerns, such as the need to control greenhouse gas emissions and to address the depletion of fossil fuel reserves, the development of new advanced materials has become a major priority. In this context, Ni–Zn alloy coatings have attracted growing interest due to their promising electrochemical properties, corrosion resistance, and potential applications in various energy-related and protective technologies. Our work focuses on the design and optimization of new Ni–Zn alloy coatings synthesized by co sputtering magnetron RF technique. In this study, Ni–Zn alloy layers (50/50 and 75/25) with target thicknesses of 50 nm and 1 μm were deposited by magnetron sputtering onto AISI 430 stainless-steel substrates. The results obtained clearly demonstrate the promising potential of Ni-rich Ni–Zn coatings for applications requiring stable, conductive, and corrosion-resistant surfaces. The main results can be summarized as follows: DS and EPMA analyses confirmed the chemical compositions of the deposited layers namely Ni-75% and Ni-50% in agreement with the targeted values. Scanning electron microscopy (SEM) of the synthesized layers revealed a relatively dense and uniform structure. XRD patterns collected for both Ni–Zn (50/50) and Ni–Zn (75/25) deposits revealed the diffraction peaks (101), (200), and (600), characteristic of the NiZn phase.XPS analysis of the two synthesized coatings allowed identification, after deconvolution, of the main high-resolution spectral regions for the following elements: Ni 2p, Ni 3p, Zn 2p, Zn 3p, C 1s, and O 1s.According to the found results, we confirm that the Nickel Zinc thin film deposited on stainless steel can be applied on different application especially on hydrogen production.

Author Statements:

- **Ethical approval:** The conducted research is not related to either human or animal use.
- **Conflict of interest:** The authors declare that they have no known competing financial interests or personal relationships that could have appeared to influence the work reported in this paper
- **Acknowledgement:**
This work was completed; thanks to the National Funds of Research DGRSDT/MESRS (Algeria). We thank researchers from researcher center of technology of semi-conductor for energetic CRTSE.
- **Author contributions:** The authors declare that they have equal right on this paper.
- **Funding information:** The authors declare that there is no funding to be acknowledged.
- **Data availability statement:** The data that support the findings of this study are available on request from the corresponding author. The data are not publicly available due to privacy or ethical restrictions.

References

1. Xia Chen, Zhengyuan Zhang, YingChen Yang, Bochen Hu, Qian Wu, Weiqiang Fan, Jinhui Hao, Weidong Shi (2024) NiCu-based catalysts with high selectivity for electro–oxidation of glucose to formic acid Chemical Engineering Science Volume 291, 5 June 2024, Page 119937
2. Chen, X., Zhang, Z., Yang, Y., Hu, B., Wu, Q., Fan, W., ... & Shi, W. (2024). NiCu-based catalysts with high selectivity for electro–oxidation of glucose to formic acid. *Chemical Engineering Science*, *291*, 119937.

3. Medrano-Banda, A., Ginoux, E., Faverge, T., Oshchepkov, A., Bonnefont, A., Chatenet, M., ... & Savinova, E. (2024). Electrochemical oxidation of glucose in alkaline environment—A comparative study of Ni and Au electrodes. Electrochimica Acta, 487, 144159.
4. Bello, I. T., Raza, H., Michael, A. T., Muneeswara, M., Tewari, N., Bingsen, W., ... & Boles, S. T. (2025). Charging Ahead: The Evolution and Reliability of Nickel-Zinc Battery Solutions. *EcoMat*, *7*(1), e12505.
5. Feng, S., Liu, J., Zhao, L., Ma, X., Liu, C., Jiang, S., ... & Yang, W. (2025). Low-Curvature Wood-Derived Thick Electrodes with High Capacity via In Situ Grown Nanoflower-Like Ni/Co Bimetallic MOFs for Aqueous Nickel–Zinc Battery. Advanced Functional Materials, e22595.
6. Zheng, L., Yi, F., Liang, J., Lu, M., Kong, J., Gao, A., & Shu, D. (2025). Construction of Low-Crystallinity Three-Dimensional Flower-like Cobalt-Doped Nickel Hydroxide for High-Performance Nickel–Zinc Batteries. ACS Applied Materials & Interfaces, 17(5), 7793-7803.
7. Sonntag, B., Dingwerth, B., Vogel, R., & Scheller, B. (2010). Cyanide formation in zinc-nickel electroplating. Galvanotechnik, 101(5), 992-996.
8. Townsend, H. E. (1991, March). Coated Steel Sheets for Corrosion-Resistant Automobiles. In CORROSION 1991 (pp. 1-20). Association for Materials Protection and Performance.
9. Divisek, J., Malinowski, P., Mergel, J., & Schmitz, H. (1988). Improved components for advanced alkaline water electrolysis. International journal of hydrogen energy, 13(3), 141-150.
10. De Giz, M. J., Machado, S. A. S., Avaca, L. A., & Gonzalez, E. R. (1992). High area Ni-Zn and Ni-Co-Zn codeposits as hydrogen electrodes in alkaline solutions. Journal of applied electrochemistry, 22(10), 973-977.
11. Sheela, G., Pushpavanam, M., & Pushpavanam, S. (2002). Zinc–nickel alloy electrodeposits for water electrolysis. International journal of hydrogen energy, 27(6), 627-633.
12. Müller, C., Sarret, M., & Benballa, M. (2001). Some peculiarities in the codeposition of zinc–nickel alloys. Electrochimica Acta, 46(18), 2811-2817.
13. Raj, I. A., & Vasu, K. I. (1992). Transition metal-based cathodes for hydrogen evolution in alkaline solution: electrocatalysis on nickel-based ternary electrolytic codeposits. Journal of applied electrochemistry, 22(5), 471-477.
14. Giridhar, J., & Van Ooij, W. J. (1992). Study of Zn-Ni and Zn-Co alloy coatings electrodeposited on steel strips II: Corrosion, dezincification and sulfidation of the alloy coatings. Surface and Coatings Technology, 53(1), 35-47.
15. Alfantazi, A. M., Page, J., & Erb, U. (1996). Pulse plating of Zn-Ni alloy coatings. Journal of applied electrochemistry, 26(12), 1225-1234.
16. Sohi, M. H., & Jalali, M. (2003). Study of the corrosion properties of zinc–nickel alloy electrodeposits before and after chromating. Journal of Materials Processing Technology, 138(1-3), 63-66.
17. Wharton, J. A., Wilcox, G. D., & Baldwin, K. R. (1996). Non-chromate conversion coating treatments for electrodeposited zinc-nickel alloys. Transactions of the IMF, 74(6), 210-213.
18. Zhang, R., Wang, X., Yu, S., Wen, T., Zhu, X., Yang, F., ... & Hu, W. (2017). Ternary NiCo2Px nanowires as pH-universal electrocatalysts for highly efficient hydrogen evolution reaction. Advanced materials, 29(9), 1605502.
19. Xie, L., Liu, Q., Shi, X., Asiri, A. M., Luo, Y., & Sun, X. (2018). Superior alkaline hydrogen evolution electrocatalysis enabled by an ultrafine PtNi nanoparticle-decorated Ni nanoarray with ultralow Pt loading. Inorganic Chemistry Frontiers, 5(6), 1365-1369.
20. Zhao, Z., Liu, H., Gao, W., Xue, W., Liu, Z., Huang, J., ... & Huang, Y. (2018). Surface-engineered PtNi-O nanostructure with record-high performance for electrocatalytic hydrogen evolution reaction. Journal of the American Chemical Society, 140(29), 9046-9050.
21. Garcés-Pineda, F. A., Blasco-Ahicart, M., Nieto-Castro, D., López, N., & Galán-Mascarós, J. R. (2019). Direct magnetic enhancement of electrocatalytic water oxidation in alkaline media. Nature Energy, 4(6), 519-525.
22. Wang, Y., Zhang, L., Yin, K., Zhang, J., Gao, H., Liu, N., ... & Zhang, Z. (2019). Nanoporous iridium-based alloy nanowires as highly efficient electrocatalysts toward acidic oxygen evolution reaction. ACS applied materials & interfaces, 11(43), 39728-39736.
23. Park, J., Sa, Y. J., Baik, H., Kwon, T., Joo, S. H., & Lee, K. (2017). Iridium-based multimetallic nanoframe@ nanoframe structure: an efficient and robust electrocatalyst toward oxygen evolution reaction. ACS nano, 11(6), 5500-5509.
24. Bar-Hen, A., Hettler, S., Ramasubramaniam, A., Arenal, R., Bar-Ziv, R., & Sadan, M. B. (2022). Catalysts for the hydrogen evolution reaction in alkaline medium: Configuring a cooperative mechanism at the Ag-Ag2S-MoS2 interface. Journal of Energy Chemistry, 74, 481-488.
25. Bayram, O., Sener, E., İgman, E. et al. Investigation of structural, morphological and optical properties of Nickel-doped Zinc oxide thin films fabricated by co-sputtering. J Mater Sci: Mater Electron **30**, 3452–3458 (2019). https://doi.org/10.1007/s10854-018-00620-2
26. Shafiq ullah, Amin Badshah, Fiaz Ahmed, Ramsha Raza, Ataf Ali Altaf, Rizwan Hussain,Electrodeposited Zinc Electrodes for High Current Zn/AgO Bipolar Batteries,International Journal of Electrochemical Science,Volume 6, Issue 9,2011,Pages 3801 3811,https://doi.org/10.1016/S1452-3981(23)18290-3.
27. Kobbi Souhila ,BADJI Mouna Sirine, Elaboration, caractérisation, et activation des couches Ni-Zn riches en Ni. Étude de leurs performances dans a

production de l'hydrogène vert, master/2024 ; USTHB.

28. Diafi, M. ., Benramache, S. , Temam, E. G. , Lakhdar, A. M. ., & Gasmi, B. . (2016). Study of Zn-Ni alloy coatings modified by nano-al2o3 particles incorporation. Acta Metallurgica Slovaca, 22(3), 171–180. https://doi.org/10.12776/ams.v22i3.706
29. Shouxu Wang, Ruiqi Shen, Cheng Yang, Yinghua Ye, Yan Hu, Chuangxin Li,Fabrication, characterization, and application in nanoenergetic materials of uncracked nano porous silicon thick films,Applied Surface Science,Volume 265,2013,Pages 4-9,https://doi.org/10.1016/j.apsusc.2012.09.148.
30. Zinc Nanoparticles at Intercrystallite Sites of (Cu0.5Tl0.5)Ba2Ca3Cu4O12−*δ*Superconductor Irfan Qasim, M. Mumtaz, K. Nadeem and S. Qamar Abbas, Journal of Nanomaterials Volume 2016, Article ID 9781790, 6 pages http://dx.doi.org/10.1155/2016/9781790
31. Yao H, Hu X, Chen Q, Wang H, Bai X. Microstructure and Corrosion Behavior of Zinc/Hydroxyapatite Multi-Layer Coating Prepared by Combining Cold Spraying and High-Velocity Suspension Flame Spraying. Materials. 2023; 16(20):6782. https://doi.org/10.3390/ma16206782
32. YAN, Xiaoqing, XIA, Mengyang, LIU, Hanxuan, *et al.* An electron-hole rich dual-site nickel catalyst for efficient photocatalytic overall water splitting. *Nature Communications*, 2023, vol. 14, no 1, p. 1741. https://doi.org/10.1038/s41467-023-37358-3
33. Habib, N., Guellati, O., Harat, A. et al. Ni–Zn hydroxide-based bi-phase multiscale porous nanohybrids: physico-chemical properties. Appl Nanosci 10, 2467–2477 (2020). https://doi.org/10.1007/s13204-019-01062-w
34. 35 Ciria-Ramos, Isabel and Tejedor, Inés and Caparros, Lucía and Doñagueda, Beatriz and Lacruz, Oscar and Urtizberea, Ainhoa and Roubeau, Olivier and Gascón, Ignacio and Haro, Marta,2023; Evaluation of triphenylene-based MOF ultrathin films for lithium batteries,Dalton Trans.52(21),pp7196-7207, doi :10.1039/D3DT00876B.
35. 36 Danhua Xu, Donghua Fan, Wenzhong Shen, 2013, Catalyst-free direct vapor-phase growth of Zn1−xCuxO micro-cross structures and their optical properties, Nanoscale Research Letters 8(1):46 DOI: 10.1186/1556-276X-8-46.
36. 37 Paromita Kundu, Nisha Singhania, Giridhar Madras, Ravishankar Narayanan ,2012, ZnO-Au nanohybrids by rapid microwave-assisted synthesis for CO oxidation June, Dalton Transactions 41(29):8762-6, DOI: 10.1039/c2dt30882g.
37. Subhashish Dey , Ganesh Chandra Dhal , Ram Prasad , Devendra Mohan (2017)Effect of nitrate metal (Ce, Cu, Mn and Co) precursors for the total oxidation of carbon monoxide, Resource-Efficient Technologies, Volume 3, Issue 3, September 2017, Pages 293-302, https://doi.org/10.1016/j.reffit.2016.12.010.
38. Varodi, C.; Pog˘acean, F.; Ciorit, ˘a, A.; Pan˘a, O.; Leos, tean, C.;Cozar, B.; Radu, T.; Coros,,M.;S, tefan-van Staden, R.I.; Pruneanu,S.-M. Nitrogen and Sulfur Co-DopedGraphene as Efficient ElectrodeMaterial for L-Cysteine Detection.Chemosensors 2021, 9, 146. https://doi.org/10.3390/chemosensors9060146.